Case Studies in Thermal Engineering 55 (2024) 104161

Contents lists available at ScienceDirect

Case Studies in Thermal Engineering

journal homepage: www.elsevier.com/locate/csite

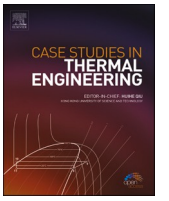

Effects of magnetohydrodynamics and velocity slip on mixed convective flow of thermally stratified ternary hybrid nanofluid over a stretching/shrinking sheet

Farah Nadzirah Jamrus [a,b], Iskandar Waini [c], Umair Khan [a,d,e], Anuar Ishak [a,*]

[a] Department of Mathematical Sciences, Faculty of Science and Technology, Universiti Kebangsaan Malaysia, 43600, UKM Bangi, Selangor, Malaysia
[b] Kolej Pengajian Pengkomputeran, Informatik dan Matematik, Universiti Teknologi MARA Cawangan Melaka Kampus Jasin, 77300, Merlimau, Melaka, Malaysia
[c] Fakulti Teknologi dan Kejuruteraan Industri dan Pembuatan, Universiti Teknikal Malaysia Melaka, Hang Tuah Jaya, 76100, Durian Tunggal, Melaka, Malaysia
[d] Department of Mathematics, Faculty of Science, Sakarya University, Serdivan, Sakarya 54050, Turkey
[e] Department of Computer Science and Mathematics, Lebanese American University, Byblos, Lebanon

ARTICLE INFO

Handling Editor: Huihe Qiu

Keywords:
MHD
Nanofluid
Heat transfer
Dual solutions
Stability analysis

ABSTRACT

This paper undertakes a numerical exploration into the dynamics of fluid flow and heat transfer within the stagnation region of a mixed convection scenario involving thermally stratified ternary hybrid nanofluid. The study incorporates the impact of a magnetohydrodynamic and velocity slip, while also considering a permeable sheet that can stretch or shrink. The equations governed the flow problem are transformed into similarity equations using a similarity transformation. Then the similarity equations are solved utilizing the built in solver (bvp4c) in MATLAB. This flow problem has two solutions, as expected. Following that, the outcomes of the stability analysis show the viability and physical robustness of the first solution. Additionally, the study identifies magnetic, suction, and volume fraction as parameters capable of delaying turbulence onset in the boundary layer. Moreover, the heat transmission of the ternary hybrid nanofluid is enhanced by an increased volume fraction. It is important to note that the reported results specifically pertain to the combination of alumina, copper, and titania nanoparticles. Different combinations of nanoparticles may exhibits unique properties related to both flow behaviour and heat transmission.

Nomenclature

Roman letters

a, b, A, B	positive constant
c	velocity ratio parameter
u, v	velocities component in the $x-$ and $y-$ directions
t	time (s)
T	temperature (k)

* Corresponding author.
E-mail address: anuar_mi@ukm.edu.my (A. Ishak).

https://doi.org/10.1016/j.csite.2024.104161
Received 15 January 2024; Received in revised form 18 February 2024; Accepted 20 February 2024
Available online 22 February 2024

B_0	constant magnetic field
S	wall mass suction parameter
M	magnetic parameter
k	thermal conductivity of the nanofluid $(W\,m^{-1}K^{-1})$
C_p	specific heat at constant pressure $(J\,kg^{-1}\,K^{-1})$
Pr	Prandtl number
Gr	Grashof number
C_f	skin friction coefficient
Nu_x	Nusselt number along $x-$ axis
Re_x	Reynold number along $x-$ axis
f	dimensionless stream function

Greek symbols

ν	kinematic viscosity $(m^2\,s^{-1})$
μ	dynamic viscosity $(kg\,m^{-1}s^{-1})$
ρ	density $(kg\,m^{-3})$
σ	electrical conductivity $(\omega^{-1}m^{-1})$
δ	thermal stratification parameter
$\mathfrak{E}$	velocity slip parameter
β_T	thermal expansion (K^{-1})
C_p	heat capacitance of the nanofluid $(J\,kg^{-1}\,K^{-1})$
φ_1	volume fraction of Al_2O_3 nanoparticle
φ_2	volume fraction of Cu nanoparticle
φ_3	volume fraction of TiO_2 nanoparticle
λ	mixed convection parameter
η	similarity variable
θ	dimensionless temperature
Γ	dimensionless time variable
γ	smallest eigenvalue

Subscripts

$s1$	for Al_2O_3 nanoparticle
$s2$	for Cu nanoparticle
$s3$	for TiO_2 nanoparticle
bf	base fluid
f	nanofluid
hnf	hybrid nanofluid
$thnf$	ternary hybrid nanofluid
w	at wall
∞	at free stream region

Superscript

’	differentiation with respect to η

1. Introduction

The capacity of fluids to transport heat is a critical characteristic in industrial and engineering applications. This characteristic is utilised in a wide array of contexts, including power generation processes and refrigeration systems in power plants, as well as chemical reactions. As heat transfer mediums, conventional fluids like water, ethylene glycol, and ethanol are typically utilised in these processes. Their thermal conductivity, however, is restricted. As a result, researchers are currently engaged in the active investigation of alternative fluids that possess improved thermal conductivity through the integration of solid particles into conventional heat transfer fluids. However, this approach faces obstacles such as the deposition of particles, obstruction in microchannel devices, and increased pressure reductions. Over the course of time, Choi and Eastman [1] made a significant advancement by developing a revolutionary fluid that they referred to as nanofluid. This fluid was distinguished by increased thermal conductivity and improved heat transfer coefficients throughout its existence. The formation of this cutting-edge fluid is accomplished by dispersing nanoparticles into a conventional fluid that serves as the base fluid. Nanofluids find application in various contexts, including heat transfer devices, thermal regulation systems for electronics, automobile radiators, refrigerating systems, and solar ponds [2–4]. Consequently, ternary hybrid nanofluid, an advanced type of nanofluid, acknowledges the significance of producing substantial improvements in the thermal conductivity of traditional fluids is introduced. The objective of this formulation is to attain an extraordinarily elevated level of heat

conductivity [5]. Theoretically, ternary hybrid nanofluid is believed to have enhanced thermal properties in contrast to single and hybrid nanofluid. Adun et al. [6] reviewed the process of creating ternary hybrid nanofluids, as well as their stabilization and their applications in heat transfer applications. In their experiment, Ahmed et al. [7] employed a square flow conduit to conduct a heat transfer experiment utilizing a ternary hybrid nanofluid composed of ZnO–Al_2O_3–TiO_2/water (zinc oxide-alumina-titania/water). The researchers confirmed that the ternary hybrid nanofluid possesses enhanced local and average heat transmission. Meanwhile, a study conducted by Kashyap et al. [8] found that using ternary hybrid nanofluid as a coolant is not beneficial due to a slight rise in the heat transfer rate. Besides experimental studies, there are quite a number of numerical studies conducted involving ternary hybrid nanofluid flow across different type of geometry and physical parameters. Algehyne et al. [9] examined how varying diffusion affects the thermal properties of ternary hybrid nanofluid. Mahmood et al. [10] performed an investigation to understand the fluid dynamics and thermal properties of ternary hybrid nanofluid flow across a stretching/shrinking curved surface in stagnation region. Sarfraz et al. [11] explored the level of energy transport in ternary hybrid nanofluid over a spiralling disk. Given the impact of radiation and Navier slip, Maranna et al. [12] investigated the flow of ternary hybrid nanofluid across a shrinking sheet in a porous media.

Stretching and shrinking surfaces are common in many real-world problems, particularly in the manufacturing industry, polymer engineering, and metallurgy [13]. Extrusion and rolling operations in manufacturing require stretching or shrinking of materials. Polymer shaping and processing may involve stretching or shrinking to achieve desired qualities in polymer engineering. Metal heat treatment and forming might entail stretching or shrinking operations in metallurgy. Consequently, these scenarios have attracted researchers to underscore the practical significance of investigating stretching and shrinking surfaces in fluid dynamics and heat transfer analyses, offering insights for understanding and optimizing operations across various sectors. In the initial exploration of this field, the idea of boundary layer flow on a solid surface moving at a constant speed was proposed by Sakiadis [14]. Subsequently, Crane [15] extended the application of boundary layer flow to two-dimensional steady flow on a stretched surface in a viscous fluid. Since then, this line of study has served as inspiration for numerous researchers exploring diverse physical aspects of boundary layer flow problems in viscous fluids on stretching/shrinking surfaces, including studies on nanofluid flow over a stretching/shrinking surfaces. For instance, Lanjwani et al. [16] explored the flow of nanofluid made of iron particles over a sheet that is being stretched or shrunk, while also considering the impact of thermal radiation. Nawaz et al. [17] introduced a study on magnetohydrodynamics (MHD) free convection flow of nanofluids over a permeable moving plate. Additionally, Abbas et al. [18] developed a mathematical model for the power-law nanofluid flow over a Riga stretching sheet and scrutinize the effect of heat generation, Brownian motion, and thermophoresis on the considered flow. In addition, the micropolar nanofluid flow over an exponentially stretching curved surface with chemical reaction, thermal slip and concentration slip effects were studied by Fuzhang et al. [19]. Meanwhile, Mahabaleshwar et al. [20] inspected the features of hybrid nanofluid flow dynamics across a stretching/shrinking sheet. They specifically focused on the joint impact of thermal radiation and mass transpiration. Ishak et al. [21] examined the magnetohydrodynamics effect on the ternary hybrid nanofluid across a stretching/shrinking sheet, incorporating gyrotactic microorganisms into their investigation.

Most of fluid flow problems are boundary value problems that are composed of nonlinear equations permitting multiple solution, which is an advantageous characteristic in engineering design and scientific research. Researchers are interested to examine these potential multiple solutions with the intention of deepening their understanding of the issue at hand or identifying solutions that satisfy specific requirements or limitations. There is a method, which is a stability analysis applied by Merkin [22] in a study of nonunique solutions in mixed convection flow within a porous media to comprehensively inspect and delineate these solutions. The author discovered that the first solution exhibits stability, whereas the second solution demonstrates instability. Following this, Weidman et al. [23] conducted a similar investigation to evaluate the reliability of the solutions as the transpiration parameter was varied. The findings are consistent with [22], affirming the viability and physical robustness of the first solution, while indicating the instability of the second solution. Since then, researcher has applied stability analysis to study the nonunique solutions of fluid flow specifically across shrinking/stretching sheet, where the solutions duality occurred because of the effect of several parameters such as suction, shrinking, and mixed convection parameters [24].

Convection is a heat transmission method assisted by fluid movement, involving heat transfer via the movement of fluid particles from a higher temperature location to one of lower temperature. Convection exists in two forms: free convection and forced convection. When the influences of forced flow from free convection and buoyant force from forced convection combine, the phenomenon is known as mixed convection, and it contributes to the total heat transfer phenomena. Solar energy systems, nuclear reactors, heat transfer devices, thermal regulation systems for electronics, and many other engineering and industrial industries rely heavily on mixed convection. Ishak et al. [25] explored the problem of stagnation region of a vertical stretched sheet using mixed convection micropolar fluid flow. It was observed that for the case of opposing flow, within a specific range of the buoyancy parameter, dual solutions were exhibited. Mixed convection stagnation point flow in Powell-Eyring fluid over a vertical permeable stretching/shrinking sheet possessed dual solutions and stability analysis was performed to identify the physically reliable solution [26]. Meanwhile, Jamaludin et al. [27] inspected the behaviour of the mixed convection flow of Cross fluid within the stagnation region past a vertical permeable shrinking sheet and executed stability analysis on the dual solutions discovered in their study. Siddiqi et al. [28] did a study on mixed convection flow in Casson fluid within the stagnation area past a stretching surface. The study involved both analytical and numerical analyses, focusing on the changes in film thickness and unsteadiness parameter. Swain et al. [24] investigated the mixed convection stagnation-point flow of a non-Newtonian third-grade fluid across a vertical permeable stretching/shrinking sheet. They utilised numerical methods to analyse the flow and conducted stability analysis to evaluate the presence of dual solutions. Lanjwani et al. [29] inspected the radiation and magnetic effects on mixed convection flow over an exponential stretching/shrinking sheet in Cassin nanofluid. They also performed stability analysis to assess the stability of the multiple solutions.

The importance of magnetohydrodynamic (MHD) flow lies in its applicability across diverse domains and its relevance in various scientific and engineering disciplines including petroleum, heating system, electrostatic mechanisms, power production, metallurgy,

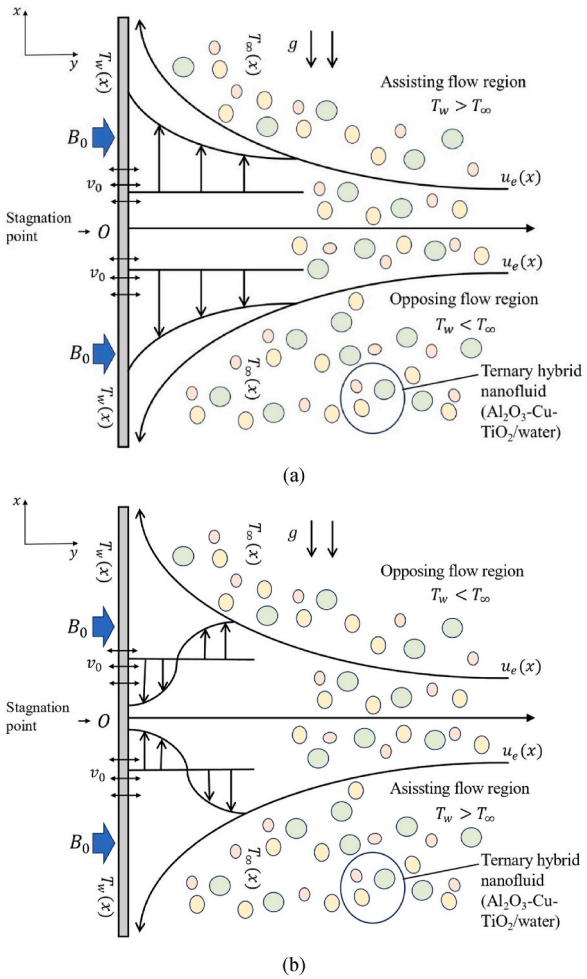

Fig. 1. Flow geometry for (a) stretching case and (b) shrinking case.

and electromagnetic pumps in aerospace and chemical processing [30]. In some industrial processes, MHD is used for controlling and manipulating the flow of conductive fluids, which can enhance heat transfer and mixing efficiency [31]. Consequently, a great number of researchers have taken an interest in this topic to investigate the influences of MHD on the heat transmission and fluid flow dynamics within a stagnation region. Nadeem et al. [32] discussed a comparative analysis focusing on different models of nanofluids. The study specifically explored unsteady oscillatory stagnation point flow of nanofluids, considering the combined effect of magnetic, Brownian motion and thermophoresis. They discovered that the flow velocity increases as the magnetic parameter increases along with the nanoparticle volume fraction. Additionally, Saleem et al. [33] inspected the heat and mass transfer in MHD Jeffrey fluid flow induced by the rotating cone under the influence of chemical reaction and heat sink/source. A related study conducted by Jamaludin et al. [34] investigated the effect of heat source/sink effect on MHD mixed convection hybrid nanofluid flow in the stagnation region over a sheet that can stretch and shrink vertically. It is clarified that opposing and assisting flows both exhibit dual solutions. It has been observed that an increase in the magnetic parameter is associated with a corresponding rise in the velocity profile and a fall in the temperature profile. In a related study, Md Ali et al. [35] looked at the two possible outcomes of MHD mixed convection stagnation point flow over a sheet that is stretching vertically, considering the effects of thermal radiation in the case of a thick fluid. Their research revealed that dual solutions only occur when there is opposing flow, whereas for assisting flow, there is only one solution. Moreover, a rise in the magnetic parameter is associated with a decline in the velocity profile. Meanwhile, Shah et al. [36] explored the similar problem but considering a vertically permeable shrinking sheet. For a specific combination of shrinking and suction parameters, dual solutions have been identified. Moreover, it was shown that the flow characteristics exhibit a reduction when the magnetic parameter increases. Besides that, MHD effect on mixed convection of a micropolar hybrid nanofluid within stagnation region over a vertical stretching/shrinking sheet, taking into account the influence of convective boundary also has been considered [37]. They found two solutions for the flow problem studied. Moreover, with an augmentation in the magnetic parameter, the velocity profile experiences a rise, whereas the temperature profile undergoes a fall.

In real-world applications, the no-slip condition cannot be assumed universally. In certain scenarios, slip conditions, including velocity slip, must be taken into account in fluid flow problems to accurately represent the behaviour of the fluid. Velocity slip refers to

the phenomenon in which the fluid in a close distance to a solid surface has a distinct velocity that differs from that of the surface. The velocity slip condition is highly relevant in technological applications. For example, the presence of velocity slip in the fluid significantly contributes to the improvement of smoothness in prosthetic heart valves and interior cavities [38]. According to Zainal et al. [39], when a slip is introduced to the interface between a fluid and a solid surface, it creates distinct flow characteristics and the forces acting on the fluid compared to scenarios where no-slip conditions prevail. In their study, Abu Bakar et al. [40] specifically examined the impact of velocity slip on the flow dynamics of a hybrid nanofluid across a shrinking sheet in a stagnation area. Their results demonstrated that a higher velocity slip corresponds to an elevated heat transfer rate. Abbas et al. [13] discovered that the increase in velocity slip causes the temperature profile of the nanofluid to climb. Saleem et al. [41] conducted a study that explored the combined effect of slips and radiation in the context of mixed convective power law fluid flow on a non-linear moving surface.

Thermal stratification occurs in flow fields when there is a temperature difference. It is characterized by the variable ambient temperature, with the understanding that ambient temperature is not assumed to be constant [42]. Understanding thermal stratification is crucial in diverse disciplines such as environmental science, ecology, and engineering, since it impacts the dispersion of heat, nutrients, and dissolved gases in water bodies and controls the movement of air masses in the atmosphere [43]. Since the presence of thermal stratification can lead to convection processes within the fluid [44], numerous studies have explored the effect of thermal stratification combined with mixed convection on fluid flows. Besthapu et al. [45] examined the mixed convection flow of thermally stratified MHD nanofluid across a sheet that was being stretched exponentially. They discovered the heat transfer rate is decreasing as the thermal stratification parameter rises. Meanwhile, thermal stratification impact on MHD mixed convection of stagnation point flow of nanofluid across a stretching sheet was studied by Mahmood et al. [46]. From the study, an observation revealed that raising the thermal stratification value resulted in higher gradients of nanofluid velocity and temperature. Currently, only a small number of research have looked at the flow properties of a thermally stratified ternary hybrid nanofluid. Rafique et al. [47] investigated how temperature stratification impacts the MHD ternary hybrid nanofluid flow over a disc that is stretching and shrinking, without the mixed convection influence. They found that a correlation exists between the growth of the thermal stratification value and the elevation in the temperature of the ternary hybrid nanofluid.

As far as the authors know, there are no published studies that look at the mixed convection flow at the stagnation point involving thermally stratified ternary hybrid nanofluid across a vertical stretching/shrinking surface. Other effects such as magnetohydrodynamics, velocity slip and suction also considered in this study. Building upon the findings from the experiment conducted by Xuan et al. [48], this study employed a ternary hybrid nanofluid (Al_2O_3–Cu–TiO_2/water), which has been demonstrated to exhibit superior thermal properties. Moreover, a distinctive aspect of this current study is the identification of dual solutions in both assisting and opposing flow scenarios. Subsequently, stability analysis is performed to determine the physical reliability of each solution.

2. Mathematical model

A stagnation flow of thermally stratified ternary hybrid nanofluid over a vertical stretching/shrinking surface is considered. The flow configuration is described in Fig. 1. The surface is shrinking/stretching with linear velocity, $u_w(x) = ax/L$ and the free stream velocity is $u_e(x) = bx/L$ where b is positive constant and L is the characteristic length of the surface. Also, the vertical surface is assumed to have a permeable structure, enabling the occurrence of a suction effect. The magnetohydrodynamics (MHD) effect is produced when a constant intensity of magnetic field, B_0 is applied perpendicular to the vertical sheet. Meanwhile, thermal stratification is a phenomenon that is taken into consideration when there is a variation in temperature either at the surface or at a distance from the surface. Thermal buoyancy force is assumed in this study to address the thermal stratification phenomenon [45,49]. The linear stratified surrounding temperature is $T_\infty(x) = T_0 + A(x/L)$ where T_0 and A is the initial surrounding temperature and constant that varied to the alter the thermal stratification strength, respectively. The variable wall temperature is $T_w(x) = T_0 + B(x/L)$ where B is a constant. The plate undergoes heating through the convection process, driven by the temperature disparity between the wall and the surrounding temperature. When dealing with a heated surface, it is presumed that $T_w(x) > T_\infty(x)$, whereas for a cooled surface (opposing flow), it is presumed $T_w(x) < T_\infty(x)$. With all of these assumptions, the equations that govern the situation are:

$$\frac{\partial u}{\partial x} + \frac{\partial v}{\partial y} = 0, \tag{1}$$

$$u\frac{\partial u}{\partial x} + v\frac{\partial u}{\partial y} = u_e\frac{\partial u_e}{\partial x} + \frac{\mu_{thnf}}{\rho_{thnf}}\frac{\partial^2 u}{\partial y^2} + \frac{\sigma_{thnf}}{\rho_{thnf}}B_0^2(u_e - u) + \frac{g(\rho\beta)_{thnf}(T - T_\infty)}{\rho_{thnf}}, \tag{2}$$

$$u\frac{\partial T}{\partial x} + v\frac{\partial T}{\partial y} = \frac{1}{(\rho C_p)_{thnf}}\left(k_{thnf}\frac{\partial^2 T}{\partial y^2}\right), \tag{3}$$

subject to:

$$u(x,0) = u_w(x) + K\frac{\partial u}{\partial y}, v(x,0) = v_0 = -S\sqrt{\frac{b\nu}{L}}, T(x,0) = T_w(x) \text{ at } y = 0, \tag{4}$$

$u(x,y) \to u_e(x), T(x,y) \to T_\infty(x)$ as $y \to \infty$.

The velocity components in $x-$ and $y-$ directions are denoted as u and v, respectively, T is the temperature of ternary hybrid nanofluid, K is the velocity slip factor and the permeable surface allows the suction effect with velocity $v_0 = -S\sqrt{\frac{b\nu}{L}}$ along the $x-$

Table 1
The thermophysical properties of hybrid nanofluid and ternary hybrid nanofluid [50,51].

Property	Ternary hybrid nanofluid	Hybrid nanofluid
Dynamic viscosity	$\mu_{thnf} = \frac{\mu_{nf}}{(1-\varphi_1)^{2.5}(1-\varphi_2)^{2.5}(1-\varphi_3)^{2.5}}$.	$\mu_{hnf} = \frac{\mu_{nf}}{(1-\varphi_1)^{2.5}(1-\varphi_2)^{2.5}}$.
Density	$\rho_{thnf} = (1-\varphi_3)\{(1-\varphi_2)[(1-\varphi_1)\rho_f + \varphi_1\rho_{s1}] + \varphi_2\rho_{s2}\} + \varphi_3\rho_{s3}$	$\rho_{hnf} = (1-\varphi_2)[(1-\varphi_1)\rho_f + \varphi_1\rho_{s1}] + \varphi_2\rho_{s2}$
Thermal conductivity	$\frac{k_{thnf}}{k_{hnf}} = \frac{k_{s3}+2k_{hnf}-2\varphi_3(k_{hnf}-k_{s3})}{k_{s3}+2k_{hnf}+\varphi_3(k_{hnf}-k_{s3})}$, $\frac{k_{hnf}}{k_{nf}} = \frac{k_{s2}+2k_{nf}-2\varphi_2(k_{nf}-k_{s2})}{k_{s2}+2k_{nf}+\varphi_2(k_{nf}-k_{s2})}$, $\frac{k_{nf}}{k_f} = \frac{k_{s1}+2k_f-2\varphi_1(k_f-k_{s1})}{k_{s1}+2k_f+\varphi_1(k_f-k_{s1})}$.	$\frac{k_{hnf}}{k_{nf}} = \frac{k_{s2}+2k_{nf}-2\varphi_2(k_{nf}-k_{s2})}{k_{s2}+2k_{nf}+\varphi_2(k_{nf}-k_{s2})}$, $\frac{k_{nf}}{k_f} = \frac{k_{s1}+2k_f-2\varphi_1(k_f-k_{s1})}{k_{s1}+2k_f+\varphi_1(k_f-k_{s1})}$.
Heat capacity	$(\rho c_p)_{thnf} = (1-\varphi_3)\{(1-\varphi_2)[(1-\varphi_1)(\rho c_p)_f + \varphi_1(\rho c_p)_{s1}] + \varphi_2(\rho c_p)_{s2}\} + \varphi_3(\rho c_p)_{s3}$	$(\rho c_p)_{thnf} = (1-\varphi_2)[(1-\varphi_1)(\rho c_p)_f + \varphi_1(\rho c_p)_{s1} + \varphi_2(\rho c_p)_{s2}]$
Electrical conductivity	$\frac{\sigma_{thnf}}{\sigma_{hnf}} = \frac{\sigma_{s3}+2\sigma_{hnf}-2\varphi_3(\sigma_{hnf}-\sigma_{s3})}{\sigma_{s3}+2\sigma_{hnf}+\varphi_3(\sigma_{hnf}-\sigma_{s3})}$, $\frac{\sigma_{hnf}}{\sigma_{nf}} = \frac{\sigma_{s2}+2\sigma_{nf}-2\varphi_2(\sigma_{nf}-\sigma_{s2})}{\sigma_{s2}+2\sigma_{nf}+\varphi_2(\sigma_{nf}-\sigma_{s2})}$, $\frac{\sigma_{nf}}{\sigma_f} = \frac{\sigma_{s1}+2\sigma_f-2\varphi_1(\sigma_f-1)}{\sigma_2+2\sigma_f+\varphi_1(\sigma_f-\sigma_2)}$.	$\frac{\sigma_{hnf}}{\sigma_{nf}} = \frac{\sigma_{s2}+2\sigma_{nf}-2\varphi_2(\sigma_{nf}-\sigma_{s2})}{\sigma_{s2}+2\sigma_{nf}+\varphi_2(\sigma_{nf}-\sigma_{s2})}$, $\frac{\sigma_{nf}}{\sigma_f} = \frac{\sigma_{s1}+2\sigma_f-2\varphi_1(\sigma_f-1)}{\sigma_2+2\sigma_f+\varphi_1(\sigma_f-\sigma_2)}$.

Table 2
Thermophysical properties values [47,49,52].

Properties	Al_2O_3	Cu	TiO_2	Water
$\rho(\mathrm{kg/m^3})$	3970	8933	4250	997.1
$C_p(\mathrm{J/kgK})$	765	385	686.2	4179
$k(\mathrm{W/mK})$	40	400	8.9538	0.613
$\sigma(\mathrm{s/m})$	35×10^6	59.6×10^6	2.6×10^6	5.5×10^{-6}
$\beta_T(\mathrm{K^{-1}})$	0.85×10^{-5}	1.67×10^{-5}	0.9×10^{-5}	21×10^{-5}
Prandtl Number, Pr	–	–	–	6.2

direction.

Table 1presented the mathematical correlations for the thermophysical properties between ternary hybrid nanofluid and hybrid nanofluid. The terms $\mu, \rho, k, \rho C_p, \beta_T$ and σ represent viscosity, density, thermal conductivity, heat capacity, thermal expansion, and electrical conductivity, respectively. Additionally, it is worth mentioning that the subscripts $thnf, hnf, nf, f, s1, s2,$ and $s3$ represent ternary hybrid nanofluid, hybrid nanofluid, nanofluid, base fluid, first, second and third nanoparticles, respectively. The corresponding symbol values for alumina (Al_2O_3), copper (Cu), and titania (TiO_2) are denoted as φ_1, φ_2 and φ_3, respectively. Meanwhile, Table 2 provides the values of thermophysical properties for Al_2O_3, Cu, TiO_2 and water as base fluid.

By reducing Eqs. (1)–(4) to ordinary differential equations via the similarity transformation, one can obtain solutions for them. Introducing the set of dimensionless variables used in this work [49]:

$$u = u_e(x)f'(\eta), v = -\sqrt{\frac{u_e(x)\nu_f}{x}}f(\eta), \theta(\eta) = \frac{T-T_\infty(x)}{T_w(x)-T_0}, \eta = y\sqrt{\frac{u_e(x)}{x\nu_f}}, \tag{5}$$

Eqs. (1)–(4) are reduced to:

$$\frac{\mu_{thnf}/\mu_f}{\rho_{thnf}/\rho_f}f''' + ff'' - f'^2 + 1 + A_1\lambda\theta + \frac{\sigma_{thnf}/\sigma_f}{\rho_{thnf}/\rho_f}M(1-f') = 0, \tag{6}$$

$$\frac{1}{Pr}\frac{k_{thnf}/k_f}{(\rho C_p)_{thnf}/(\rho C_p)_f}\theta'' + f\theta' - (\theta+\delta)f' = 0, \tag{7}$$

subject to boundary conditions:

$$f(0) = S, f'(0) = c + \Sigma f''(0), \theta(0) = 1-\delta, \tag{8}$$

$f'(\eta)\to 1, \theta(\eta)\to 0$ as $\eta\to\infty$

where Pr is the Prandtl number, S is the wall mass suction parameter ($S > 0$), $M = \frac{\sigma_f B_0^2 L}{\rho_f b}$ is the magnetic parameter, $\Sigma = K\sqrt{\frac{b}{\nu_f L}}$ is the

velocity slip parameter, $\delta = \frac{A}{B}$ is the thermal stratification parameter, and $c = \frac{a}{b}$ is the velocity ratio parameter ($c > 0$ for stretching sheet, $c < 0$ for shrinking sheet), Meanwhile $\lambda = Gr/Re_x^2$ is the mixed convection (buoyancy) parameter where $\lambda < 0$ refers to opposing flow, $\lambda > 0$ refers to assisting flow and $\lambda = 0$ for the forced convection flow where $Gr = g(\beta_T)_f(T_w(x) - T_0)x^3/\nu_f^2$ is the Grashof number, $A_1 = \frac{(1-\varphi_3)\{(1-\varphi_2)[(1-\varphi_1)\rho_f+\varphi_1(\rho\beta_T)_{s1}/(\beta_T)_f]+\varphi_2(\rho\beta_T)_{s2}/(\beta_T)_f\}+\varphi_3(\rho\beta_T)_{s3}/(\beta_T)_f}{(1-\varphi_3)\{(1-\varphi_2)[(1-\varphi_1)\rho_f+\varphi_1\rho_{s1}]+\varphi_2\rho_{s2}\}+\varphi_3\rho_{s3}}$ and $Re_x = xu_e(x)/\nu_f$ is the local Reynolds number.

The skin friction coefficient and the local Nusselt number denote as

$$C_f = \frac{\tau_w}{\rho_f u_e^2(x)}, Nu_x = \frac{xq_w}{k_f(T_w(x) - T_0)}, \tag{9}$$

with τ_w is the surface shear stress and q_w is the surface heat flux given by

$$\tau_w = \mu_{thnf}\left(\frac{\partial u}{\partial y}\right)_{y=0}, q_w = -k_{thnf}\left(\frac{\partial T}{\partial y}\right)_{y=0}, \tag{10}$$

By applying (5) and (10) into (9), the physical quantities of interest, which are the reduced skin friction coefficient, and the heat transfer rate are obtained:

$$Re_x^{1/2}C_f = \frac{\mu_{thnf}}{\mu_f}f''(0), Re_x^{-1\backslash/2}Nu_x = -\frac{k_{thnf}}{k_f}\theta'(0) \tag{11}$$

3. Stability analysis

The property of ordinary differential equations to admit multiple solutions, often called dual solutions, which include both the first and second solutions, is widely recognised. It is not possible to experimentally identify these multiple solutions [53]. Because of this, multiple solution identification makes use of mathematical analysis. After the identification of multiple solutions, it is critical to conduct a stability test to determine their stability and instability [22,23]. Stability analysis encompasses the examination of irregular flows, characterized by time-dependent flow states. The objective of this approach is to introduce a disturbance into the time-independent flow, and the stable solution is recognised as the one that varies in time with the least amount of error.

To initiate the stability analysis, it is necessary to consider the unsteady formulation of Eqs. (2) and (3).

$$\frac{\partial u}{\partial t} + u\frac{\partial u}{\partial x} + v\frac{\partial u}{\partial y} = u_e\frac{\partial u_e}{\partial x} + \frac{\mu_{thnf}}{\rho_{thnf}}\frac{\partial^2 u}{\partial y^2} + \frac{\sigma_{thnf}}{\rho_{thnf}}B_0^2(u_e - u) + \frac{g(\rho\beta)_{thnf}(T - T_\infty)}{\rho_{thnf}}, \tag{12}$$

$$\frac{\partial T}{\partial t} + u\frac{\partial T}{\partial x} + v\frac{\partial T}{\partial y} = \frac{1}{(\rho C_p)_{thnf}}\left(k_{thnf}\frac{\partial^2 T}{\partial y^2}\right), \tag{13}$$

Then, the dimensionless time variable, denoted as Γ and a new set of dimensionless variables in term of η and Γ are introduced as follows:

$$u = u_e(x)f'(\eta,\Gamma), v = -\sqrt{\frac{u_e(x)\nu_f}{x}}f(\eta,\Gamma)$$

$$\theta(\eta,\Gamma) = \frac{T - T_\infty(x)}{T_w(x) - T_0}, \eta = y\sqrt{\frac{u_e(x)}{x\nu_f}}, \Gamma = \frac{b}{L}t \tag{14}$$

The dimensionless variables in (14) are utilised in Eqs. (12) and (13). Hence, the following system of equations are obtained:

$$\frac{\mu_{thnf}/\mu_f}{\rho_{thnf}/\rho_f}\frac{\partial^3 f}{\partial\eta^3} + f\frac{\partial^2 f}{\partial\eta^2} - \left(\frac{\partial f}{\partial\eta}\right)^2 + 1 + A\lambda\theta - \frac{\partial^2 f}{\partial\eta\partial\Gamma} + \frac{\sigma_{thnf}/\sigma_f}{\rho_{thnf}/\rho_f}M\left(1 - \frac{\partial f}{\partial\eta}\right) = 0, \tag{15}$$

$$\frac{1}{Pr}\frac{k_{thnf}/k_f}{(\rho C_p)_{thnf}/(\rho C_p)_f}\frac{\partial^2\theta}{\partial\eta^2} + f\frac{\partial\theta}{\partial\eta} - (\theta + \delta)\frac{\partial f}{\partial\eta} - \frac{\partial\theta}{\partial\Gamma} = 0, \tag{16}$$

along with the boundary conditions:

$$f(0,\Gamma) = \mathrm{S}, \frac{\partial f}{\partial\eta}(0,\Gamma) = \mathrm{c} + \mathfrak{E}\frac{\partial^2 f}{\partial\eta^2}(0,\Gamma), \theta(0,\Gamma) = 1 - \delta$$

$$\frac{\partial f}{\partial\eta}(\eta,\Gamma) \to 1, \theta(\eta,\Gamma) \to 0, \text{as } \eta\to\infty \tag{17}$$

Next, the following perturbation functions are utilised to assess the stability of the dual solutions [54]:

$$f(\eta,\Gamma) = f_0(\eta) + e^{-\gamma\Gamma}F(\eta), \theta(\eta,\Gamma) = \theta_0(\eta) + e^{-\gamma\Gamma}G(\eta), \tag{18}$$

Table 3
$f''(0)$ when $S = M = \delta = \mathfrak{E} = c = 0$ and $\lambda = 1$ for viscous fluid ($\varphi_1 = \varphi_2 = \varphi_3 = 0$)

Pr	Rostami et al. [57] (bvp4c)		Khashi'ie et al. [49] (bvp4c)		Mahmood et al. [46] (shooting method & RKF)		Present results (bvp4c)	
	1st Solution	2nd Solution	1st Solution	2nd Solution	1st Solution	2nd Solution	1st Solution	2nd Solution
0.7	1.7063	1.2344	1.7063	1.2387	1.72608	–	1.706323	1.238728
1	1.6754	1.1296	1.6754	1.1332	1.71179	–	1.675437	1.133292
7	1.5179	0.5815	1.5179	0.5824	1.57524	–	1.517913	0.582401

Table 4
$-\theta(0)$ when $S = M = \delta = \mathfrak{E} = c = 0$ and $\lambda = 1$ for viscous fluid ($\varphi_1 = \varphi_2 = \varphi_3 = 0$)

Pr	Rostami et al. [57] (bvp4c)		Khashi'ie et al. [49] (bvp4c)		Mahmood et al. [46] (shooting method & RKF)		Present results (bvp4c)	
	1st Solution	2nd Solution	1st Solution	2nd Solution	1st Solution	2nd Solution	1st Solution	2nd Solution
0.7	0.7641	1.0235	0.7641	1.0226	1.68677	–	0.764063	1.022631
1	0.8708	1.1706	0.8708	1.1691	1.69536	–	0.870779	1.169126
7	1.7224	2.2203	1.7224	2.2192	1.86382	–	1.722382	2.219294

with assumption $f_0(\eta) = f(\eta)$ and $\theta_0(\eta) = \theta(\eta)$ are the solutions for the steady state similarity equations (6) and (7) constrained by the boundary conditions (8). While $F(\eta)$ and $G(\eta)$ are assumed to be relatively small towards $f_0(\eta)$ and $\theta_0(\eta)$. Additionally, γ is the unknown eigenvalue parameter, introduced to quantify the rate at which the disturbance to the steady flow similarity equations either grows or decays. Implementing (18), Eqs. (15) and (16) and the boundary conditions (17) become

$$\frac{\mu_{thnf}/\mu_f}{\rho_{thnf}/\rho_f}F''' + f_0F'' - \left(\frac{\sigma_{thnf}/\sigma_f}{\rho_{thnf}/\rho_f}M - 2f_0' + \gamma\right)F' + f_0''F + A\lambda G = 0, \tag{19}$$

$$\frac{1}{Pr}\frac{k_{thnf}/k_f}{(\rho C_p)_{thnf}/(\rho C_p)_f}G'' + F\theta_0' + f_0G' - (\theta - \delta)F' - (f_0' - \gamma)G = 0, \tag{20}$$

with the boundary conditions:

$$F(0) = 0, F'(0) - \mathfrak{E}F''(0) = 0, G(0) = 0$$

$$F'(\eta) \to 0, G(\eta) \to 0, \text{as } \eta \to \infty \tag{21}$$

Rather than directly use $F'(\eta) \to 0$, we choose to relax this condition by replacing it with $F''(0) = 1$, allowing us to address the eigenvalue problem. Consequently, new boundary conditions for Eq. (21) are formulated:

$$F(0) = 0, F'(0) - \mathfrak{E}F''(0) = 0, F''(0) = 1, G(0) = 0$$

$$G(\eta) \to 0, \text{as } \eta \to \infty \tag{22}$$

When the eigenvalue problem is solved using the bvp4c solver, it is possible to obtain an endless number of eigenvalues. The negative eigenvalue represents the early rise of disturbance, which indicates an unstable flow over time. On the other hand, a positive eigenvalue indicates that the disturbance decreases over time, indicating a stable flow.

4. Results and discussion

The mathematical model that builds up from Eqs. (6) and (7), are actively solved using the bvp4c solver in MATLAB software while adhering to the specified boundary conditions (8). This numerical solver is widely employed in mathematics and engineering for solving boundary value problems (BVPs) associated with ordinary differential equations. This solver uses a finite difference method that employs the three-stage Lobatto IIIa formula with 4th order accuracy. In this study, solutions are sought at both the upper and lower limits by establishing a boundary layer thickness denoted as η_∞ at 15, which is sufficient to satisfy the far-field boundary conditions in an asymptotic manner. Meanwhile a tolerance threshold 10^{-10} is implemented to regulate the solver's precision and determine when it converged to a satisfactory solution. The current problem may have dual solutions, therefore the bvp4c solver requires initial guesses. These initial guesses are chosen through a trial-and-error process and are iteratively refined if solver convergence is not achieved. Finding the first solution is straightforward, even when bvp4c is provided with a weak initial guess. However, obtaining a suitable initial guess for the second solution poses a challenge. In this case, a continuation method is used to overcome this challenge [55]. As the existence of dual solutions is anticipated, a thorough stability analysis is conducted to assess the stability of the obtained solutions.

This study involves the synthesis of a ternary hybrid nanofluid by dispersing φ_1 (Al_2O_3) and φ_2 (Cu) nanoparticles into water as the base fluid. Subsequently, φ_3 (TiO_2) is introduced as the third nanoparticle, with varying volume fractions. It is important to note that in

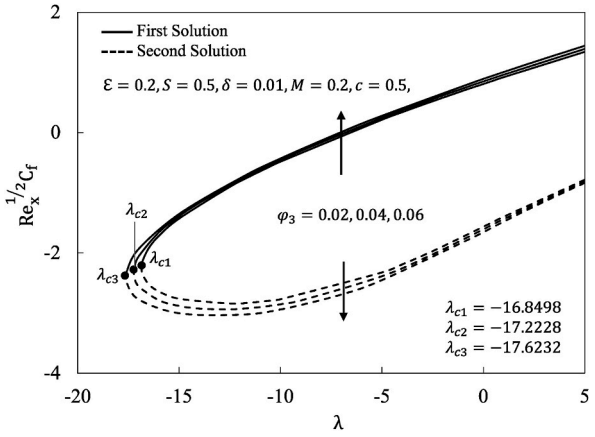

Fig. 2. Changes in skin friction against mixed convection parameter for various values of φ_3.

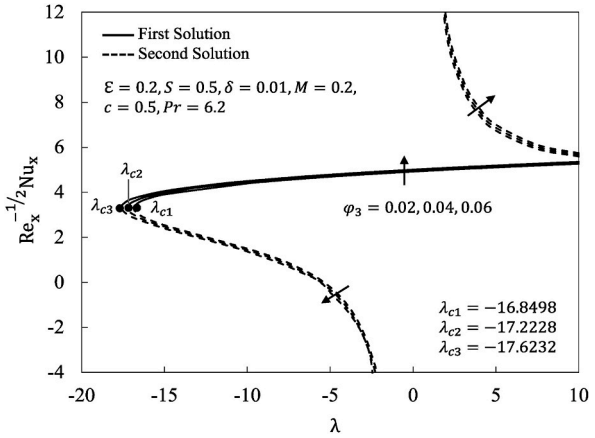

Fig. 3. Changes in Nusselt number against mixed convection parameter for various values of φ_3.

this study, φ_1 and φ_2 are fixed at 2% while $2\% \leq \varphi_3 \leq 6\%$ for the third nanoparticle. According to Oztop and Abu Nada [56], Prandtl number for water as the base fluid is $Pr = 6.2$, which is used for the entire study. This study seeks to offer a succinct analysis of the impact of various parameters such as the velocity slip Ɛ, magnetic M, stretching/shrinking c, mixed convection λ, suction S, and volumetric concentration of nanoparticles φ_3, have on fluid flow profiles, heat transfer rate, and skin friction coefficient. To achieve this objective, the selection of parameter values relies on insights from prior studies and a trial-and-error approach, thereby ensuring the presence of dual solutions.

Tables 3 and 4 depict the values of $f''(0)$ and $-\theta(0)$ for regular viscous fluid when all parameters are zero except $\lambda = 1$. The previous authors employed various methods to obtain these values, and it is evident from the tables that the results obtained from this study align exceptionally well. This consistency validates the accuracy of the numerical approach employed, thereby establishing the obtained results as accurate and reliable.

4.1. *Effect of volume fraction* φ3

Figs. 2 and 3 depict the influence of the volume fraction of nanoparticles along with mixed convection parameter on $Re_x^{1/2}C_f$ and $Re_x^{-1/2}Nu_x$. Fig. 2 depicts that increasing value of φ_3 led to the small increase of skin friction coefficient values for the first solution. Furthermore, the second solution involves augmenting the values of φ_3 causes a lessening of skin friction coefficient values. In a physical sense, elevating the volume fraction of nanoparticles results in improved fluid viscosity performance, heightened surface shear stress, and an augmentation of local skin friction. Moreover, the magnitude of $|\lambda_c|$ demonstrates an increase with a rise in the volume fraction φ_3, indicating that increasing φ_3 postpones the boundary layer detachment. Meanwhile, Fig. 3 depicts the inclination of thermal transfer efficiency along with the increasing value of φ_3 for the first solution. Yet, regarding the second solution, thermal transfer efficiency decreases under opposing flow conditions and increases under assisting flow conditions. Physically, enhancing φ_3 leads to a higher concentration of solid nanoparticles in the fluid, subsequently enhancing thermal transmission. As a result, the Nusselt number has also been augmented. This discovery aligns with a prior study conducted by Sohut et al. [37]. Furthermore, this discovery indicates that increased volume concentration can boost the heat transfer of ternary hybrid nanofluid.

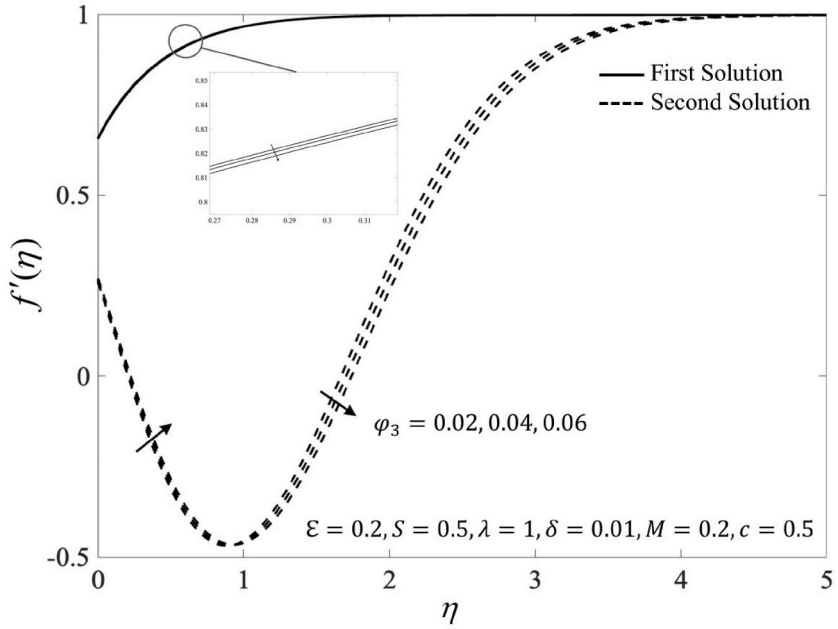

Fig. 4. Velocity profile for various values of φ_3 in the case of stretching flow.

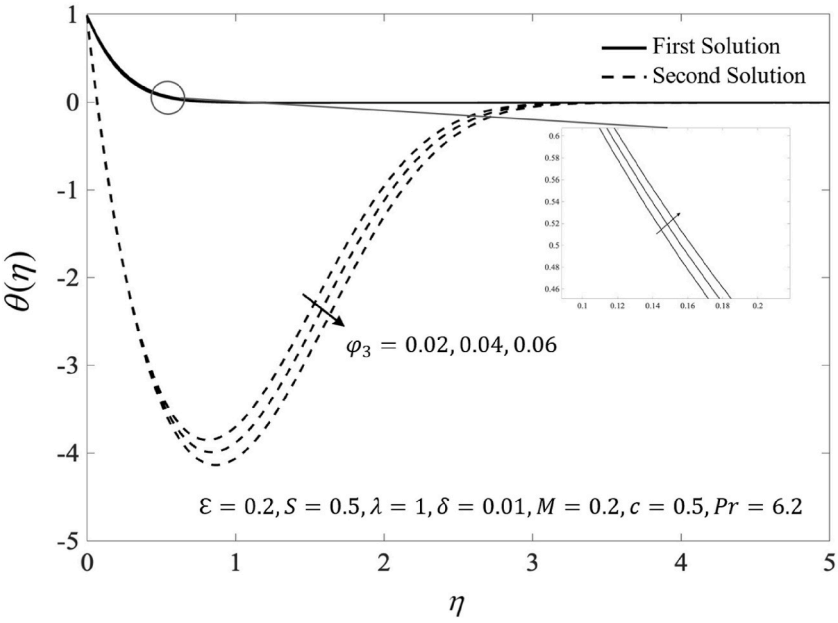

Fig. 5. Temperature profile for various values of φ_3 in the case of stretching flow.

Next, Figs. 4–7 illustrate the impact of volume fraction φ_3 on flow profiles for both a stretching and shrinking sheet. In Figs. 4 and 6, discernible trend is noted: as φ_3 increases, the velocity profiles in the first solution experience a slight decrease, while in the second solution, the decrease is more pronounced. From a physical standpoint, an elevated quantity of solid nanoparticles leads to a rise in the fluid's viscosity. With an increase in viscosity, the resistance also experiences a greater surge. As a consequence, the fluid flow is slowed. Simultaneously, in relation to temperature distributions, the fluid temperature rises in the first solution whereas in the second solution, it decreases. Augmenting the volume fraction of solid nanoparticles may generate additional energy, thereby enhancing the temperature profile.

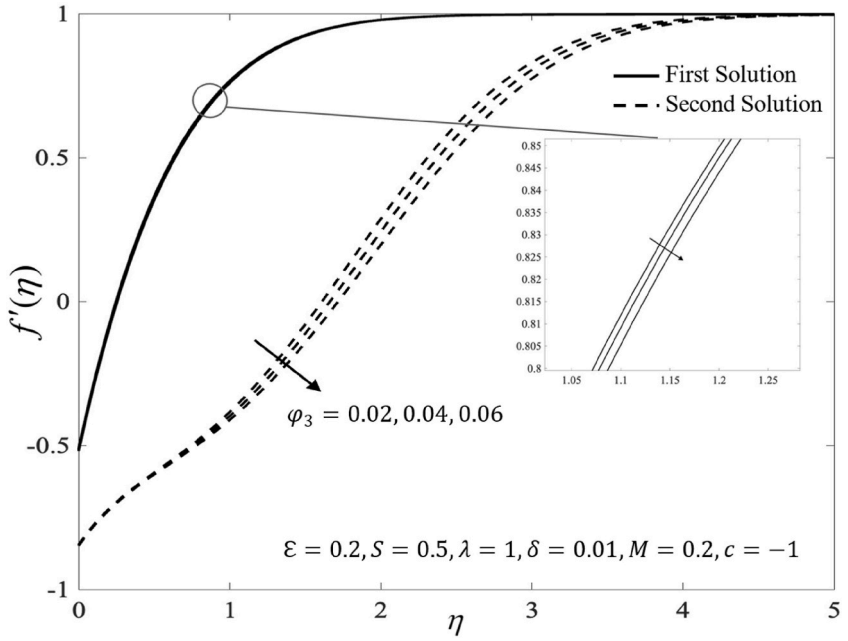

Fig. 6. Velocity profile for various values of φ_3 in the case of shrinking flow.

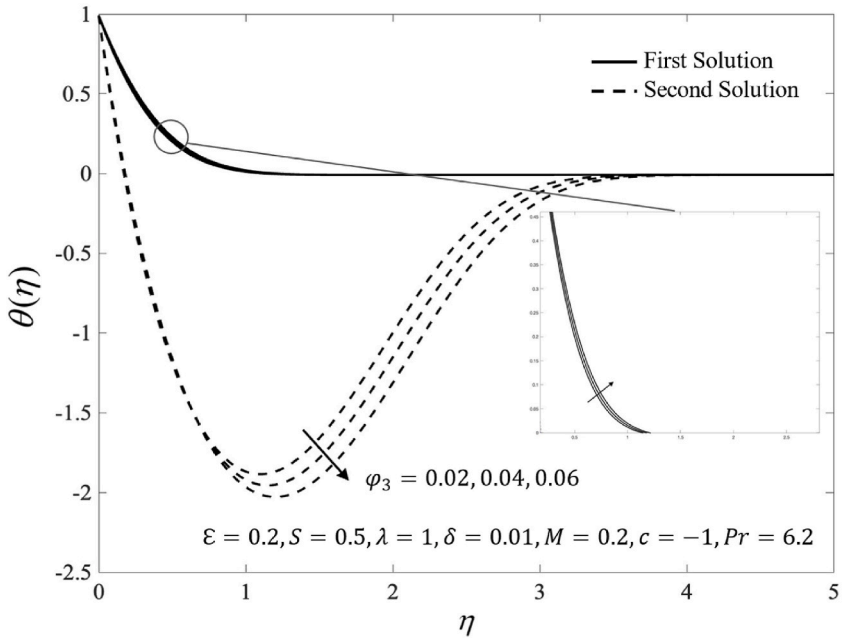

Fig. 7. Temperature profile for various values of φ_3 in the case of shrinking flow.

4.2. *Effect of the magnetic parameter*

Figs. 8 and 9 show the variation in $Re_x^{1/2}C_f$ and $Re_x^{-1/2}Nu_x$ as the magnetic parameter is varied. Skin friction and heat transfer coefficients show an upward trend in the first solution with the rise of the magnetic parameter. However, for the second solution, these physical quantities exhibit the opposite behaviour. The occurrence of these phenomena can be attributed to the Lorentz force, which generates a drag force capable of potentially modifying surface heat transfer and skin friction. Furthermore, the figures illustrate that the critical values of λ for the following values of $M = 0$, 0.2, 0.4 and 0.6 are $\lambda_c = -19.2120$, -19.9154, -20.6063, -21.2882, respectively. From a physical view, the solution range of λ is expanding. As a result, augmenting the magnetic parameter value may potentially postpone the separation of the boundary layer.

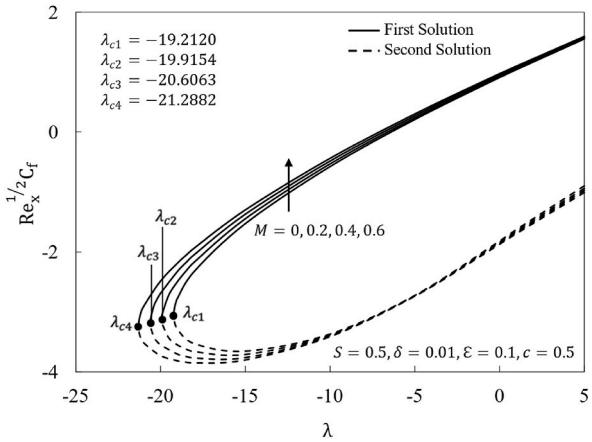

Fig. 8. Changes in skin friction against mixed convection parameter for some values of *M*.

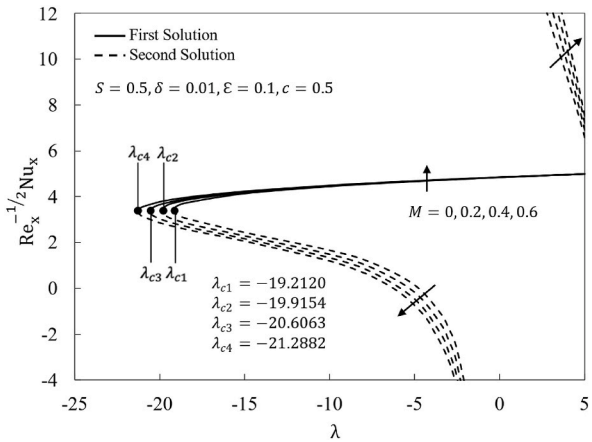

Fig. 9. Changes in Nusselt number against mixed convection parameter for some values of *M*.

Meanwhile, the impact of the magnetic parameter on the fluid profiles when $\mathcal{E} = 0.1, S = 0.5, \lambda = 1, \delta = 0.01, c = 0.5$ and $Pr = 6.2$ is illustrated in Figs. 10 and 11. The escalation of the Lorentz force is driven by an elevation in the magnetic parameter, leading to heightened momentum within the boundary layer. Consequently, the observed phenomenon induces an increase in the flow velocity at the surface. Specifically, it implies that adjusting the magnetic parameter can potentially prevent the occurrence of turbulent flow in the fluid. This result aligns with what is illustrated in Fig. 8. The increase of magnetic parameter gives the reduction in fluid temperature for the first solution and decrease for the second solution, as seen in Fig. 11. Also, the thermal boundary layer become thinner and the increase in the surface temperature gradient are found to be influenced by the Lorentz force. Physically, when a magnetic field engages with an electrically conductive nanofluid results in a drag force referred to as the Lorentz force.

4.3. *Effect of velocity slip parameter* $\mathcal{E}$

Fig. 12 illustrates skin friction coefficient values in the negative range when $\lambda < -6.6289$ in the case of an opposing direction. Meanwhile, at $\lambda = -6.6289$, the skin friction is zero, where it means at this point occurs no slip condition. Further, for $\lambda > -6.6289$, it is found that presence of velocity slip has opposed the stretching effect, then positive values of skin friction coefficients reduce. From a physical perspective, the velocity slip within the boundary layer serves to mitigate the friction between the surface and the fluid, thereby leading to a decrease in surface shear stress. In contrast, Fig. 13 shows that the inclusion of velocity slip parameter enhance the rate of heat transmission. Additionally, from both figures, we can see that an increase in the velocity slip parameter, it speeds up the separation of the boundary layer. In simpler terms, changes in this parameter make the boundary layer separate more quickly.

Further, impacts of velocity slip on the flow profiles when $S = 0.5, \lambda = 1, \delta = 0.01, M = 0.2, c = 0.5$ and $Pr = 6.2$ are shown in Figs. 14 and 15. Looking at Fig. 14, the velocity slip parameter has a notable impact on both the thickness of the momentum boundary layer and the shape of the velocity profile. The boundary layer thickness decreases, hence, the fluid velocity is increasing. Fig. 15 illustrates the reduction in temperature becoming less significant as the velocity slip parameter increases. In term of thermal boundary layer, one can observe that the velocity slip parameter gives only small reduction in its thickness.

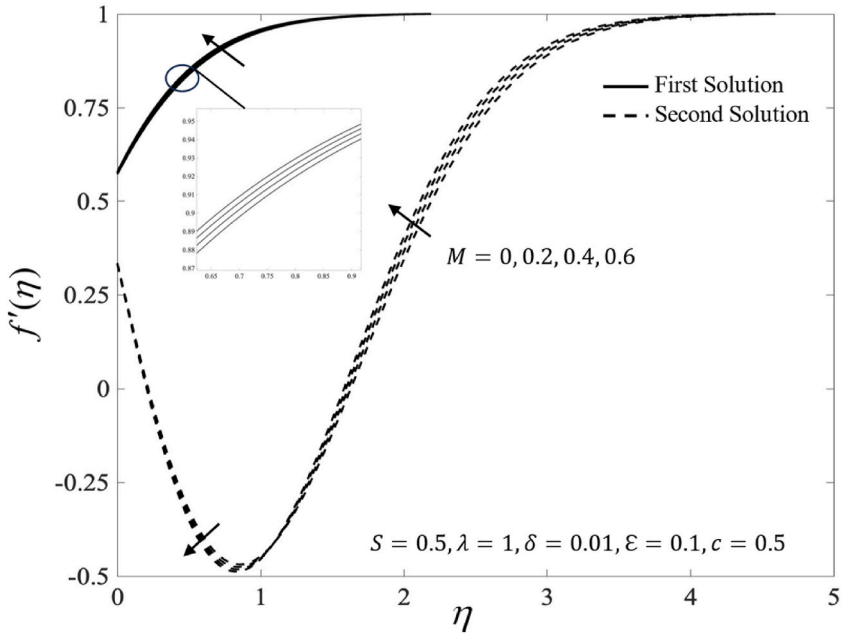

Fig. 10. Velocity profile for some values of *M*.

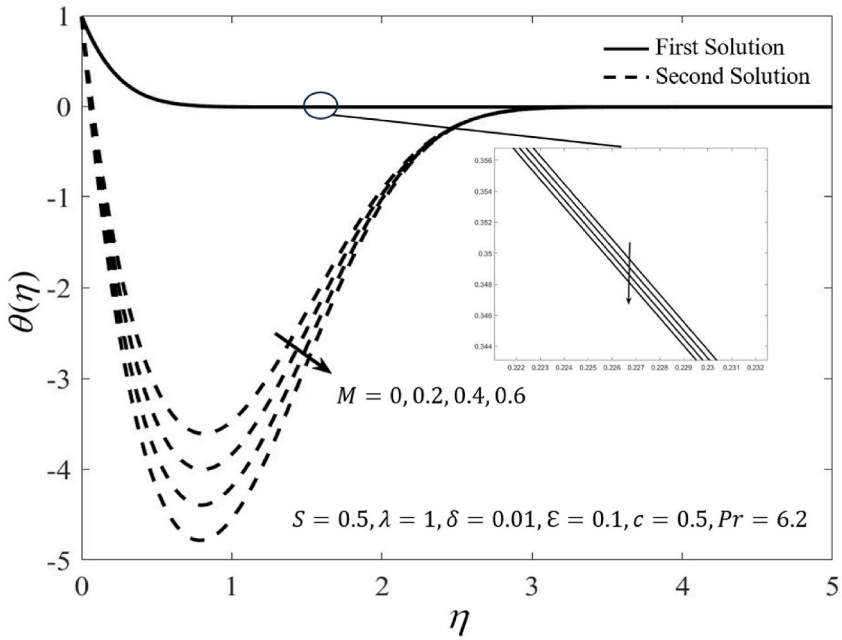

Fig. 11. Temperature profile for some values of *M*.

4.4. Effect of the suction parameter S

The increase in the suction parameter value has an impact on the acceleration of the suction velocity on the permeable surface, subsequently leading to a greater volume of nanofluid being drawn into the plate. Therefore, the suction effect becomes more pronounced with an increasing suction parameter value. Figs. 16 and 17 illustrate how the suction parameter affect $Re_x^{1/2}C_f$ and $Re_x^{-1/2}Nu_x$. The figures reveal the skin friction and thermal transfer coefficients incline for the first solution when the suction parameter is strengthened. However, the pattern shows otherwise for the second solution. Physically, the suction effect results in a larger volume of ternary hybrid nanofluid being drawn to the surface, leading to the thinning of the boundary layer. Consequently, the increase in fluid velocity causes both the skin friction coefficient and heat transfer rate to rise. Observe that in these figures, the values of $|\lambda_c|$ rise

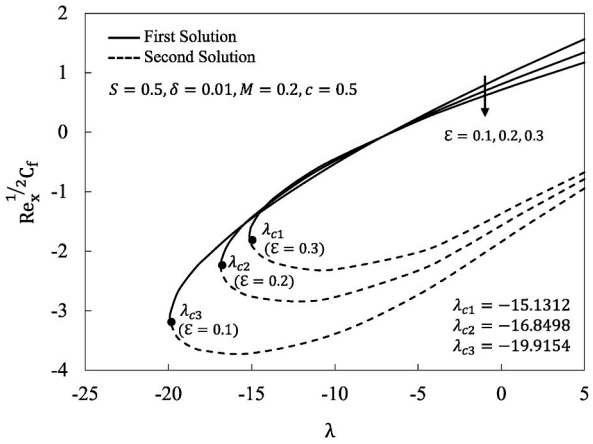

Fig. 12. Changes in skin friction for some values of ε.

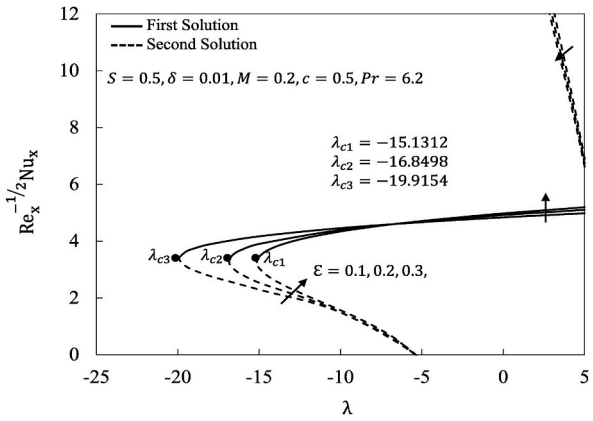

Fig. 13. Changes in Nusselt number for some values of ε.

with the escalation of the suction values, suggesting that suction parameter can widen the range of dual solutions occurrence. Therefore, suction parameter also can serve as a controlling factor for either delaying or accelerating the boundary layer detachment. Additionally, these findings are aligned with the remarkable work by Jamaludin et al. [58].

4.5. *Effect of the thermal stratification parameter δ*

Figs. 18 and 19 illustrate how skin friction and heat transfer rate are affected by the thermal stratification parameter. Increasing thermal stratification parameter expands the solution range of the problem, as indicated by the rising values of $|\lambda_c|$ in both figures. Moreover, thermal stratification parameter can delay the boundary layer detachment. Additionally, the impact of thermal stratification on surface shear stress is apparent, resulting in an increase in the skin friction coefficient values for the first solution. Rate of heat transmission also increase alongside the thermal stratification parameter in the first solution. When the thermal stratification parameter increases, a temperature difference emerges between the surface and the surrounding environment. This temperature gradient initiates the heat convection process, where heat transfers from colder to hotter regions. Consequently, with a higher thermal stratification value, convection occurs more efficiently, leading to an increased heat transfer rate.

The smallest eigenvalues γ for different values of λ with $\varepsilon = 0.1, S = 0.5, \delta = 0.01, M = 0.2, c = 0.5$ and $Pr = 6.2$ are illustrated in Fig. 20. Utilizing the definition provided by Eq. (18), negative eigenvalues correspond to early rise of disturbance, indicating long-term flow instability. Conversely, positive eigenvalues signify a reduction in disturbance over time, characterizing a stable state. Hence, evidently that the first solution exhibits a positive value for γ, whereas the second solution demonstrates a negative γ. Simultaneously, noting that the eigenvalue approaches zero for both the first and second solutions as the value approaches the critical value $\lambda_c = -19.9154$. This discovery indicates that there is a transition in the eigenvalues at the bifurcation point when they change from positive (indicating stability) to negative (indicating instability). This finding supports the conclusions drawn from the stability analysis performed in this study, indicating that the first solution is probably stable than the second solution.

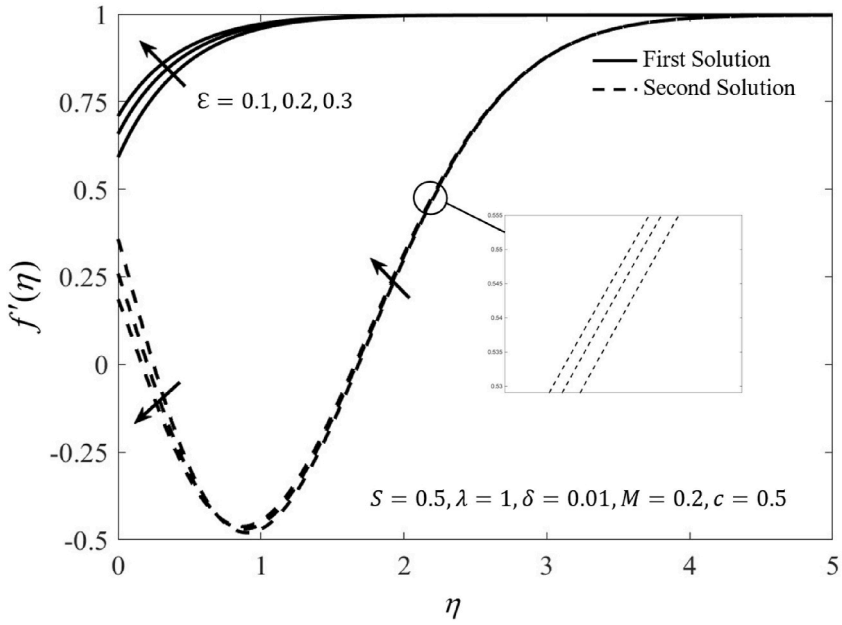

Fig. 14. Velocity profile for some values of Ɛ.

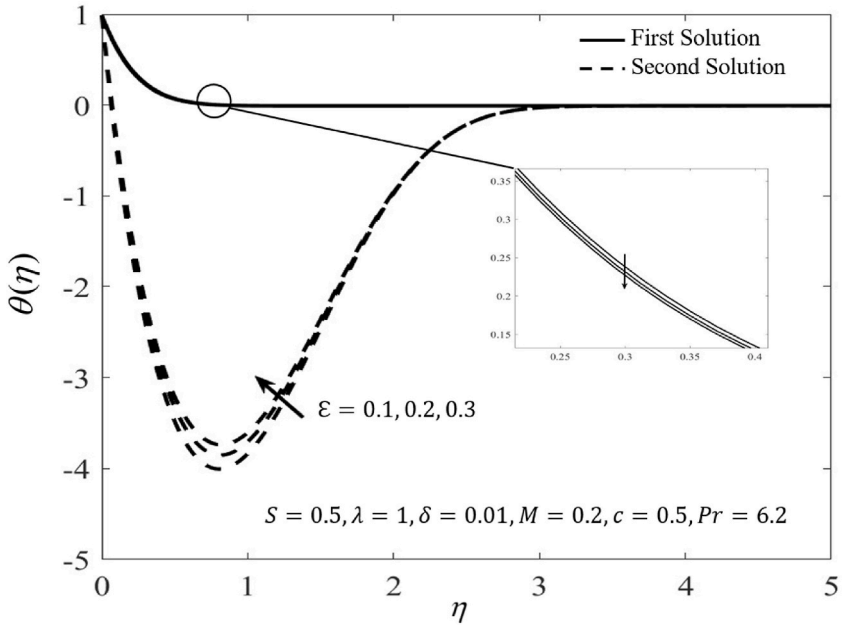

Fig. 15. Temperature profile for some values of Ɛ.

5. Conclusion

The mixed convection stagnation point flow of a thermally stratified Al_2O_3–Cu–TiO_2/water ternary hybrid nanofluid over a vertical stretching/shrinking sheet is numerically assessed in this study. The analysis considers the occurrence of a magnetic field, velocity slip, and suction. The study yielded several noteworthy discoveries.

- The numerical findings demonstrated a significant increase in heat transfer rate approximately 1.74% as the concentration of TiO_2 is raised from 2% to 6%. Additionally, the escalation in nanoparticle volume fraction amplifies fluid viscosity and shear stress at the surface, ultimately contributing to an augmented skin friction approximately over 7.42%.

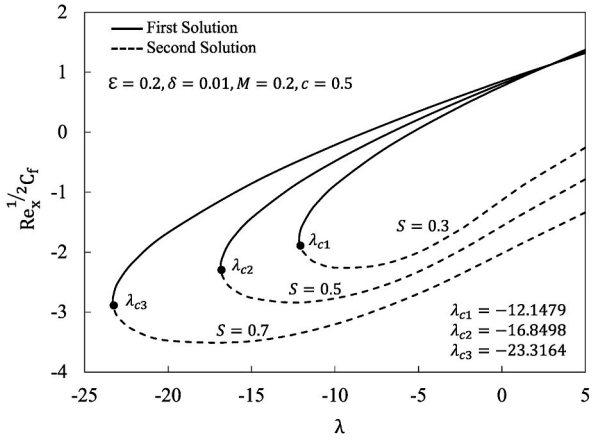

Fig. 16. Changes in skin friction for some values of S.

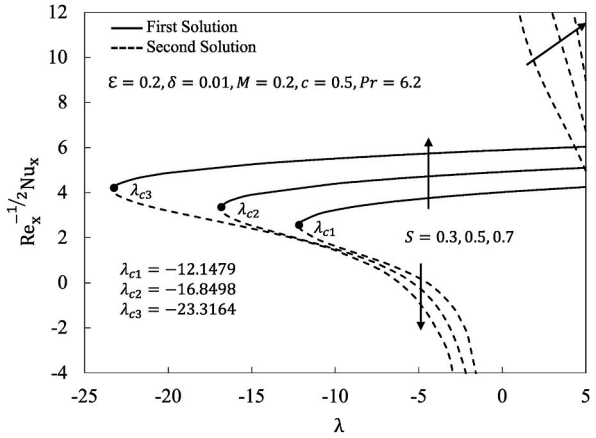

Fig. 17. Changes in Nusselt number for some values of S.

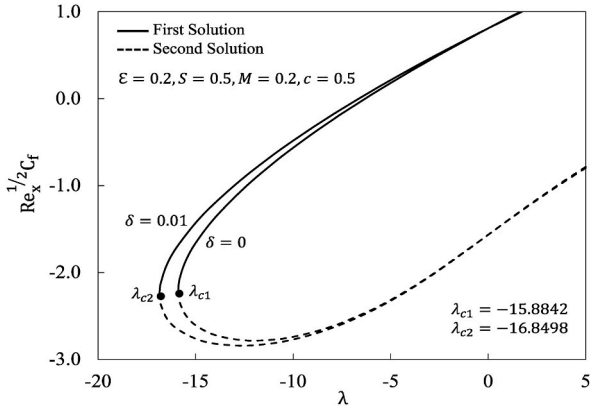

Fig. 18. Changes in skin friction for some values of δ.

- Compared to the flow scenario without magnetic effect, the Nusselt number demonstrates a marginal increase approximately 0.07% when $M = 0.2$, 0.14% when $M = 0.4$, and 0.21% when $M = 0.6$ in both assisting and opposing flow cases.
- As suction strength is elevated from 0.3 to 0.7, a noteworthy augmentation of 41.96% is observed in the heat transfer rate. This observation indicates that even with a relatively low suction strength, heat transfer rate is enhanced significantly.

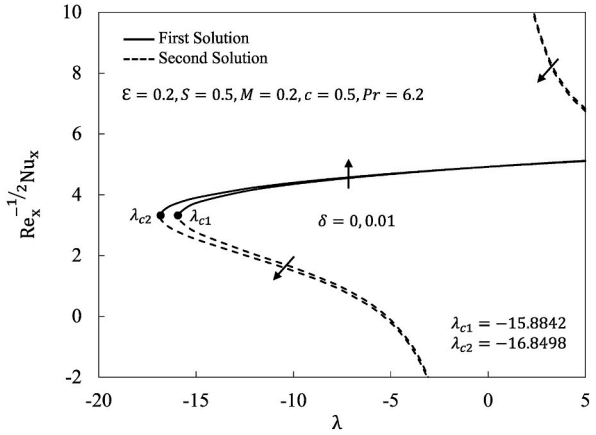

Fig. 19. Changes in Nusselt number for some values of δ.

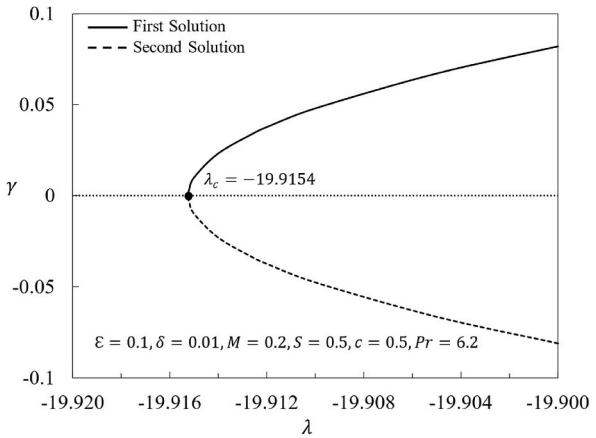

Fig. 20. Smallest eigenvalues towards mixed convection parameter.

- The parameters of magnetism, suction, and volume fraction play a critical role in delaying the boundary layer detachment, providing a method to regulate and postpone the onset of turbulence in the boundary layer.
- Dual solutions emerge in assisting and opposing flow zones.
- The stability analysis indicated that the stability of the first solution confirmed and exhibits physical robustness.

CRediT authorship contribution statement

Farah Nadzirah Jamrus: Writing – original draft, Methodology, Investigation. **Iskandar Waini:** Writing – review & editing, Validation, Supervision, Methodology, Conceptualization. **Umair Khan:** Writing – review & editing, Validation, Methodology, Investigation. **Anuar Ishak:** Writing – review & editing.

Declaration of competing interest

The authors declare that they have no known competing financial interests or personal relationships that could have appeared to influence the work reported in this paper.

Data availability

No data was used for the research described in the article.

Acknowledgement

The authors would like to acknowledge Universiti Teknikal Malaysia Melaka (PJP/2022/FTKMP/S01891) and Universiti Kebangsaan Malaysia (DIP-2023-005) for the financial supports.

References

[1] S.U.S. Choi, J.A. Eastman, Enhancing thermal conductivity of fluids with nanoparticles, Proceedings of the, FED, ASME International Mechanical Engineering Congress and Exposition 231 (66) (1995) 99–105, 1995.
[2] S.K. Gupta, A. Sharma, A brief review of nanofluids utilization in heat transfer devices for energy saving, Mater. Today: Proceedings, Mar. (2023), https://doi.org/10.1016/j.matpr.2023.03.364.
[3] L.S. Sundar, Synthesis and characterization of hybrid nanofluids and their usage in different heat exchangers for an improved heat transfer rates: a critical review, Engineering Science and Technology, an International Journal 44 (Aug. 2023) 101468, https://doi.org/10.1016/j.jestch.2023.101468.
[4] G. Goga, et al., Heat transfer enhancement in solar pond using nano fluids, Mater. Today: Proceedings, Jan. (2023), https://doi.org/10.1016/j.matpr.2022.12.238.
[5] V. Puneeth, et al., Implementation of modified Buongiorno's model for the investigation of chemically reacting rGO-Fe3O4-TiO2-H2O ternary nanofluid jet flow in the presence of bio-active mixers, Chem. Phys. Lett. 786 (2022) 139194, https://doi.org/10.1016/j.cplett.2021.139194.
[6] H. Adun, D. Kavaz, M. Dagbasi, Review of ternary hybrid nanofluid: synthesis, stability, thermophysical properties, heat transfer applications, and environmental effects, J. Clean. Prod. 328 (Dec. 2021) 129525, https://doi.org/10.1016/j.jclepro.2021.129525.
[7] W. Ahmed, et al., Heat transfer growth of sonochemically synthesized novel mixed metal oxide ZnO+Al2O3+TiO2/DW based ternary hybrid nanofluids in a square flow conduit, Renew. Sustain. Energy Rev. 145 (2021) 111025, https://doi.org/10.1016/j.rser.2021.111025.
[8] S. Kashyap, J. Sarkar, A. Kumar, Performance enhancement of regenerative evaporative cooler by surface alterations and using ternary hybrid nanofluids, Energy 225 (Jun. 2021) 120199, https://doi.org/10.1016/j.energy.2021.120199.
[9] E.A. Algehyne, H.F. Alrihieli, M. Bilal, A. Saeed, W. Weera, Numerical approach toward ternary hybrid nanofluid flow using variable diffusion and non-Fourier's concept, ACS Omega 7 (33) (Aug. 2022) 29380–29390, https://doi.org/10.1021/acsomega.2c03634.
[10] Z. Mahmood, U. Khan, S. Saleem, K. Rafique, S.M. Eldin, Numerical analysis of ternary hybrid nanofluid flow over a stagnation region of stretching/shrinking curved surface with suction and Lorentz force, J. Magn. Magn Mater. 573 (May 2023) 170654, https://doi.org/10.1016/j.jmmm.2023.170654.
[11] M. Sarfraz, M. Khan, A. Al-Zubaidi, S. Saleem, Enhancing energy transport in Homann stagnation-point flow over a spiraling disk with ternary hybrid nanofluids, Case Stud. Therm. Eng. 49 (Sep. 2023) 103134, https://doi.org/10.1016/j.csite.2023.103134.
[12] T. Maranna, U.S. Mahabaleshwar, L.M. Pérez, O. Manca, Flow of viscoelastic ternary nanofluid over a shrinking porous medium with heat Source/Sink and radiation, Therm. Sci. Eng. Prog. 40 (May 2023) 101791, https://doi.org/10.1016/j.tsep.2023.101791.
[13] I. Abbas, S. Hasnain, N.A. Alatawi, M. Saqib, D.S. Mashat, Thermal radiation energy performance on stagnation-point flow in the presence of base fluids ethylene glycol and water over stretching sheet with slip boundary condition, Energies 15 (21) (Oct. 2022) 7965, https://doi.org/10.3390/en15217965.
[14] B.C. Sakiadis, Boundary-layer behavior on continuous solid surfaces: I. Boundary-layer equations for two-dimensional and axisymmetric flow, AIChE J. 7 (1) (Mar. 1961) 26–28, https://doi.org/10.1002/aic.690070108.
[15] L.J. Crane, Flow past a stretching plate, Zeitschrift für angewandte Mathematik und Physik ZAMP 21 (4) (Jul, 1970) 645–647, https://doi.org/10.1007/BF01587695.
[16] H.B. Lanjwani, M.S. Chandio, K. Malik, M.M. Shaikh, Stability analysis of boundary layer flow and heat transfer of Fe2O3 and Fe-water base nanofluid over a stretching/shrinking sheet with radiation effect, Eng. Technol. Appl. Sci. Res. 12 (1) (Feb. 2022) 8114–8122, https://doi.org/10.48084/etasr.4649.
[17] M. Nawaz, U. Nazir, S. Saleem, S.O. Alharbi, An enhancement of thermal performance of ethylene glycol by nano and hybrid nanoparticles, Phys. Stat. Mech. Appl. 551 (Aug. 2020) 124527, https://doi.org/10.1016/j.physa.2020.124527.
[18] N. Abbas, K.U. Rehman, W. Shatanawi, K. Abodayeh, Mathematical Model of Temperature-dependent Flow of Power-Law Nanofluid over a Variable Stretching Riga Sheet, *Waves in Random and Complex Media*, Aug. 2022, pp. 1–18, https://doi.org/10.1080/17455030.2022.2111029.
[19] W. Fuzhang, M.I. Anwar, M. Ali, A.S. El-Shafay, N. Abbas, R. Ali, Inspections of Unsteady Micropolar Nanofluid Model over Exponentially Stretching Curved Surface with Chemical Reaction, Waves in Random and Complex Media, Feb. 2022, pp. 1–22, https://doi.org/10.1080/17455030.2021.2025280.
[20] U.S. Mahabaleshwar, A.B. Vishalakshi, H.I. Andersson, Hybrid nanofluid flow past a stretching/shrinking sheet with thermal radiation and mass transpiration, Chin. J. Phys. 75 (Jan. 2022) 152–168, https://doi.org/10.1016/j.cjph.2021.12.014.
[21] S.S. Ishak, Mohd Rijal Ilias, Seripah Awang Kechil, Ternary hybrid nanofluids containing gyrotactic microorganisms with magnetohydrodynamics effect over a shrinking/stretching of the horizontal plate, Journal of Advanced Research in Fluid Mechanics and Thermal Sciences 109 (2) (Nov. 2023) 102–230, https://doi.org/10.37934/arfmts.109.2.210230.
[22] J.H. Merkin, On dual solutions occurring in mixed convection in a porous medium, J. Eng. Math. 20 (2) (1986) 171–179, https://doi.org/10.1007/BF00042775.
[23] P.D. Weidman, D.G. Kubitschek, A.M.J. Davis, The effect of transpiration on self-similar boundary layer flow over moving surfaces, Int. J. Eng. Sci. 44 (11–12) (Jul. 2006) 730–737, https://doi.org/10.1016/j.ijengsci.2006.04.005.
[24] S. Swain, G.M. Sarkar, B. Sahoo, Dual solutions and linear temporal stability analysis of mixed convection flow of non-Newtonian special third grade fluid with thermal radiation, Int. J. Therm. Sci. 189 (Jul. 2023) 108262, https://doi.org/10.1016/j.ijthermalsci.2023.108262.
[25] A. Ishak, R. Nazar, I. Pop, Mixed convection stagnation point flow of a micropolar fluid towards a stretching sheet, Meccanica 43 (4) (Aug. 2008) 411–418, https://doi.org/10.1007/s11012-007-9103-5.
[26] K. Naganthran, R. Nazar, I. Pop, A study on non-Newtonian transport phenomena in a mixed convection stagnation point flow with numerical simulation and stability analysis, The European Physical Journal Plus 134 (3) (Mar. 2019) 105, https://doi.org/10.1140/epjp/i2019-12454-0.
[27] A. Jamaludin, R. Nazar, I. Pop, Mixed convection stagnation-point flow of Cross fluid over a shrinking sheet with suction and thermal radiation, Phys. Stat. Mech. Appl. 585 (Jan. 2022) 126398, https://doi.org/10.1016/j.physa.2021.126398.
[28] M. Tanzeel-ur-Rehman Siddiqi, et al., Comparative analysis of analytical and numerical approximations for the flow and heat transfer in mixed convection stagnation point flow of Casson fluid, Results Phys. 52 (Sep. 2023) 106819, https://doi.org/10.1016/j.rinp.2023.106819.
[29] H.B. Lanjwani, S. Saleem, M.S. Chandio, M.I. Anwar, N. Abbas, Stability analysis of triple solutions of Casson nanofluid past on a vertical exponentially stretching/shrinking sheet, Adv. Mech. Eng. 13 (11) (Nov. 2021) 168781402110596, https://doi.org/10.1177/16878140211059679.
[30] M.I. Anwar, H. Firdous, A.A. Zubaidi, N. Abbas, S. Nadeem, Computational analysis of induced magnetohydrodynamic non-Newtonian nanofluid flow over nonlinear stretching sheet, Prog. React. Kinet. Mech. 47 (2022) 146867832110727, https://doi.org/10.1177/14686783211072712.
[31] N.S. Khashi'ie, I. Waini, A.R.M. Kasim, N.A. Zainal, A. Ishak, I. Pop, Magnetohydrodynamic and viscous dissipation effects on radiative heat transfer of non-Newtonian fluid flow past a nonlinearly shrinking sheet: Reiner–Philippoff model, Alex. Eng. J. 61 (10) (Oct. 2022) 7605–7617, https://doi.org/10.1016/j.aej.2022.01.014.
[32] S. Nadeem, A.U. Khan, S. Saleem, A comparative analysis on different nanofluid models for the oscillatory stagnation point flow, The European Physical Journal Plus 131 (8) (Aug. 2016) 261, https://doi.org/10.1140/epjp/i2016-16261-9.
[33] S. Saleem, M.M. Al-Qarni, S. Nadeem, N. Sandeep, Convective heat and mass transfer in magneto Jeffrey fluid flow on a rotating cone with heat source and chemical reaction, Commun. Theor. Phys. 70 (5) (Nov. 2018) 534, https://doi.org/10.1088/0253-6102/70/5/534.
[34] A. Jamaludin, K. Naganthran, R. Nazar, I. Pop, MHD mixed convection stagnation-point flow of Cu-Al2O3/water hybrid nanofluid over a permeable stretching/shrinking surface with heat source/sink, Eur. J. Mech. B Fluid 84 (Nov. 2020) 71–80, https://doi.org/10.1016/j.euromechflu.2020.05.017.
[35] F. Md Ali, A.N.A. Khamat, M.M. Junoh, Dual solutions in mixed convection stagnation-point flow over a vertical stretching sheet with external magnetic field and radiation effect, Journal of Advanced Research in Fluid Mechanics and Thermal Sciences 80 (2) (Feb. 2021) 22–32, https://doi.org/10.37934/arfmts.80.2.2232.
[36] S.H.A.M. Shah, M. Suleman, U. Khan, Dual solution of MHD mixed convection flow and heat transfer over a shrinking sheet subject to thermal radiation, Partial Differential Equations in Applied Mathematics 6 (Dec. 2022) 100412, https://doi.org/10.1016/j.padiff.2022.100412.
[37] F. Sohut, A. Ishak, S. Soid, MHD stagnation point of blasius flow for micropolar hybrid nanofluid toward a vertical surface with stability analysis, Symmetry (Basel) 15 (4) (Apr. 2023) 920, https://doi.org/10.3390/sym15040920.

[38] M.M. Khader, A.M. Megahed, Numerical solution for boundary layer flow due to a nonlinearly stretching sheet with variable thickness and slip velocity, The European Physical Journal Plus 128 (9) (Sep. 2013) 100, https://doi.org/10.1140/epjp/i2013-13100-7.
[39] N.A. Zainal, R. Nazar, K. Naganthran, I. Pop, Unsteady stagnation point flow of hybrid nanofluid past a convectively heated stretching/shrinking sheet with velocity slip, Mathematics 8 (10) (Sep. 2020) 1649, https://doi.org/10.3390/math8101649.
[40] S. Abu Bakar, N. Md Arifin, N.S. Khashi'ie, N. Bachok, Hybrid nanofluid flow over a permeable shrinking sheet embedded in a porous medium with radiation and slip impacts, Mathematics 9 (8) (Apr. 2021) 878, https://doi.org/10.3390/math9080878.
[41] S. Saleem, M. Abd El-Aziz, Entropy generation and convective heat transfer of radiated non-Newtonian power-law fluid past an exponentially moving surface under slip effects, The European Physical Journal Plus 134 (4) (Apr. 2019) 184, https://doi.org/10.1140/epjp/i2019-12656-4.
[42] N.S. Khashi'ie, E. Hafidz Hafidzuddin, N. Md Arifin, N. Wahi, CFD letters stagnation point flow of hybrid nanofluid over a permeable vertical stretching/shrinking cylinder with thermal stratification effect, CFD Lett. 12 (2020) 80–94.
[43] T. Hayat, M. Farooq, A. Alsaedi, Thermally stratified stagnation point flow of Casson fluid with slip conditions, Int. J. Numer. Methods Heat Fluid Flow 25 (4) (May 2015) 724–748, https://doi.org/10.1108/HFF-05-2014-0145.
[44] S. Mukhopadhyay, I.C. Mondal, R.S.R. Gorla, Effects of thermal stratification on flow and heat transfer past a porous vertical stretching surface, Heat Mass Tran. 48 (6) (Jun. 2012) 915–921, https://doi.org/10.1007/s00231-011-0930-5.
[45] P. Besthapu, R.U. Haq, S. Bandari, Q.M. Al-Mdallal, Mixed convection flow of thermally stratified MHD nanofluid over an exponentially stretching surface with viscous dissipation effect, J. Taiwan Inst. Chem. Eng. 71 (Feb. 2017) 307–314, https://doi.org/10.1016/j.jtice.2016.12.034.
[46] Z. Mahmood, S.E. Alhazmi, A. Alhowaity, R. Marzouki, N. Al-Ansari, U. Khan, MHD mixed convective stagnation point flow of nanofluid past a permeable stretching sheet with nanoparticles aggregation and thermal stratification, Sci. Rep. 12 (1) (Sep. 2022) 16020, https://doi.org/10.1038/s41598-022-20074-1.
[47] K. Rafique, et al., Investigation of thermal stratification with velocity slip and variable viscosity on MHD flow of Al2O3-Cu-TiO2/H2O nanofluid over disk, Case Stud. Therm. Eng. 49 (Sep. 2023) 103292, https://doi.org/10.1016/j.csite.2023.103292.
[48] Z. Xuan, Y. Zhai, M. Ma, Y. Li, H. Wang, Thermo-economic performance and sensitivity analysis of ternary hybrid nanofluids, J. Mol. Liq. 323 (Feb. 2021) 114889, https://doi.org/10.1016/j.molliq.2020.114889.
[49] N.S. Khashi'ie, N.M. Arifin, N. Wahi, N. Md Arifin, E. Hafidz Hafidzuddin, I. Pop, Mixed convective stagnation point flow of a thermally stratified hybrid Cu-Al_2O_3/water nanofluid over a permeable stretching/shrinking sheet, ASM Science Journal 12 (5) (2019) 17–25. https://www.researchgate.net/publication/337828593.
[50] S. Manjunatha, V. Puneeth, B.J. Gireesha, A.J. Chamkha, Theoretical study of convective heat transfer in ternary nanofluid flowing past a stretching sheet, Journal of Applied and Computational Mechanics 8 (4) (2022) 1279–1286, https://doi.org/10.22055/JACM.2021.37698.3067.
[51] S.P.A. Devi, S.S.U. Devi, Numerical investigation of hydromagnetic hybrid Cu - Al2O3/water nanofluid flow over a permeable stretching sheet with suction, Int. J. Nonlinear Sci. Numer. Stimul. 17 (5) (Aug. 2016) 249–257, https://doi.org/10.1515/ijnsns-2016-0037.
[52] P.M. Patil, M. Kulkarni, Analysis of MHD mixed convection in a Ag-TiO_2 hybrid nanofluid flow past a slender cylinder, Chin. J. Phys. 73 (Oct. 2021) 406–419, https://doi.org/10.1016/j.cjph.2021.07.030.
[53] J. Raza, Similarity Solutions of Boundary Layer Flows in a Channel Filled by Non-newtonian Fluids, PhD Thesis, Universiti Utara Malaysia, Changlun, Malaysia, 2018.
[54] P. Weidman, M.R. Turner, Stagnation-point flows with stretching surfaces: a unified formulation and new results, Eur. J. Mech. B Fluid 61 (Jan. 2017) 144–153, https://doi.org/10.1016/j.euromechflu.2016.09.019.
[55] L.F. Shampine, I. Gladwell, S. Thompson, Solving ODEs with MATLAB, first ed., Cambridge University Press, 2003 https://doi.org/10.1017/CBO9780511615542.
[56] H.F. Oztop, E. Abu-Nada, Numerical study of natural convection in partially heated rectangular enclosures filled with nanofluids, Int. J. Heat Fluid Flow 29 (5) (Oct. 2008) 1326–1336, https://doi.org/10.1016/j.ijheatfluidflow.2008.04.009.
[57] M.N. Rostami, S. Dinarvand, I. Pop, Dual solutions for mixed convective stagnation-point flow of an aqueous silica–alumina hybrid nanofluid, Chin. J. Phys. 56 (5) (Oct. 2018) 2465–2478, https://doi.org/10.1016/j.cjph.2018.06.013.
[58] A. Jamaludin, R. Nazar, I. Pop, Mixed convection stagnation-point flow of a nanofluid past a permeable stretching/shrinking sheet in the presence of thermal radiation and heat source/sink, Energies 12 (5) (Feb. 2019) 788, https://doi.org/10.3390/en12050788.